基于二氧化钒宽、窄带可切换的双功能超材料吸收器研究

封覃银 裘国华 严德贤 李吉宁 李向军

Wide and narrow band switchable bi-functional metamaterial absorber based on vanadium dioxide

FENG Qin-yin, QIU Guo-hua, YAN De-xian, Li Ji-ning, Li Xiang-jun

---

您可能感兴趣的其他文章

Articles you may be interested in

电环形谐振腔表面几何参数对太赫兹超材料吸收体性能的影响

Influence of the geometric parameters of the electrical ring resonator metasurface on the performance of metamaterial absorbers for terahertz applications

中国光学. 2018, 11(1): 47   https://doi.org/10.3788/CO.20181101.0047

变换光学透镜天线研究进展

Research progress of transformation optics lens antenna

中国光学. 2017, 10(2): 164   https://doi.org/10.3788/CO.20172002.0164

太赫兹偏振测量系统及其应用

Polarization sensitive terahertz measurements and applications

中国光学. 2017, 10(1): 98   https://doi.org/10.3788/CO.20171001.0098

铕掺杂纳米二氧化钛透明光触媒乳液的制备及光催化性能研究

Preparation of europium−doped nano−TiO_2 transparent photocatalyst emulsion and photocatalytic performance

中国光学. 2017, 10(6): 760   https://doi.org/10.3788/CO.20171006.0760

超快激光制备生物医用材料表面功能微结构的现状及研究进展

Surface functional microstructure of biomedical materials prepared by ultrafast laser: a review

中国光学. 2019, 12(2): 199   https://doi.org/10.3788/CO.20191202.0199

电磁编码超材料的理论与应用

Theory and application of coding metamaterials

中国光学. 2017, 10(1): 1   https://doi.org/10.3788/CO.20171001.0001

Wide and narrow band switchable bi-functional metamaterial absorber based on vanadium dioxide

FENG Qin-yin[1], QIU Guo-hua[1]*, YAN De-xian[1]*, Li Ji-ning[2], Li Xiang-jun[1]

（1. *Key Laboratory of Electromagnetic Wave Information Technology and Metrology of Zhejiang Province,*
College of Information Engineering, China Jiliang University, Hangzhou 310018, *China*;

2. *College of Precision Instrument and Optoelectronic Engineering, Tianjin University, Tianjin* 300072, *China*）
* *Corresponding author*, *E-mail*: *qghfr@163.com*; *yandexian*1991*@cjlu.edu.cn*

Abstract: A wide-band and narrow-band switchable bi-functional metamaterial absorber is presented in this paper. The phase change material vanadium dioxide (VO_2) is introduced in the structure of the metamaterial absorber, and different functions can be achieved by using only a single switchable metasurface. The mutual conversion of different functions is realized by the reversible phase transition between the VO_2 insulating state and the metal state. When VO_2 is in metallic state, the designed structure can be regarded as a metamaterial wide-band absorber. The simulation results show that the absorption is over 98% in the frequency range of 1.55 THz to 2.21 THz. When VO_2 is in the insulating state, the structure acts as a narrow-band absorber, and the absorption at resonance frequencies of 2.54, 2.93 and 3.34 THz is over 95%. In addition, the effect of geometric parameters on the absorption of metamaterial absorber is discussed. Because of the symmetry of the element structure, the absorber is insensitive to the polarization when the electromagnetic wave is vertically incident, and it can keep good absorption performance with the large incident angle. Therefore, the switchable bi-functional metamaterial absorber proposed in this paper can be widely used in terahertz modulation, thermal emitters and electromagnetic energy acquisition, etc.

Key words: metamaterial; vanadium dioxide; bi-function; absorber

基于二氧化钒宽、窄带可切换的
双功能超材料吸收器研究

封覃银[1],裘国华[1*],严德贤[1*],李吉宁[2],李向军[1]

（1. 中国计量大学 信息工程学院 浙江省电磁波信息技术与计量检测重点实验室，
杭州 310018；

2. 天津大学 精密仪器与光电子工程学院，天津 300072）

摘要：本文提出了一种宽、窄带可切换的双功能超材料吸收器。在超材料吸收器的结构中，引入了相变材料二氧化钒（VO_2），仅利用单个可切换超表面就能实现不同的功能，其不同功能之间的相互转换通过 VO_2 绝缘态和金属态之间的可逆相变特性实现。当 VO_2 处于金属态时，设计的结构可以看作一个超材料宽带吸收器。仿真结果表明，在 1.55THz 至 2.21THz 的宽带频率范围内，吸收率超过 98%。当 VO_2 处于绝缘态时，该结构作为窄带吸收器，在共振频率 2.54THz、2.93THz 和 3.34THz 处的吸收率在 95% 以上，实现了完美吸收。此外，还讨论了几何参数对超材料吸收器吸收率性能的影响。由于单元结构的对称性，该吸收器在电磁波垂直入射时具有极化不敏感特性，并且在大入射角范围内仍能保持良好的吸收性能。因此，本文提出的可切换双功能超材料吸收器可广泛应用于太赫兹调制、热发射器和电磁能量采集等各种领域。

关　键　词：超材料；二氧化钒；双功能；吸收器

1　Introduction

Terahertz wave (THz wave) mainly refers to electromagnetic wave with frequency between 0.1 THz and 10 THz, which is located between microwave and infrared light wave[1]. In recent years, with the rapid development of terahertz detection technology and time-domain spectroscopy technology, terahertz wave detection, modulation and other related technologies have attracted more and more attention[2]. Metamaterials are a new type of artificially designed electromagnetic composites that have attracted great interest in many potential applications, such as terahertz absorbers[3-4], polarization converters[5], sensors[6]. In recent years, many researchers have proposed a variety of the terahertz-based metamaterial absorber models, and studied their single frequency band[7], multi-frequency band[8-10] and wide frequency band[11-12] characteristics. As a functional device that can achieve high absorptivity of incident electromagnetic wave[13-14], metamaterial absorber has promising application

prospects[18-19] in many fields such as infrared detection[15], modern communication, electromagnetic stealth[16], thermal radiation, and sensing[17]. The early terahertz absorber has a single resonance mode and narrow absorption spectrum bandwidth. Most designed metamaterial absorption devices can only achieve a single function at the working frequency or cannot tune the absorption performance according to the application requirements. Various shortcomings limit its practical application.

With the emergence of functional materials (phase change materials) such as graphene[20-21], liquid crystals (LC)[22], and vanadium dioxide (VO_2)[23], it is possible to change the properties of materials simply by applying excitations such as electricity[24-25], magnetism, light[26], and temperature[27]. Combining these functional materials with metamaterial structures allows multiple functions to be implemented in a single metamaterial device, thus driving the rapid development of terahertz metamaterial absorbers. VO_2, as an excellent phase change material, has optical and electrical properties that

change significantly during the phase change, and the conductivity can change by 4−5 orders of magnitude[23], making it ideal for tunable multifunctional metamaterial device. Liu[23] *et al*. proposed a VO$_2$-based ultra-wideband absorber that can achieve modulation of 5% to 80% absorption in the wideband range of 1.2 to 3.2 THz. Song[28] *et al*. proposed the design of a VO$_2$-based terahertz wideband tunable absorber, by which the amplitude of the wide-band absorption band can be adjusted from 5% to 96% when the VO$_2$ conductivity changes from 10 S/m to 2000 S/m. Zhang[29] *et al*. proposed a terahertz bi-functional absorber with wide-band and narrow-band absorption characteristics based on a graphene/spacer-VO$_2$/spacer-metal structure. The operating bandwidth and intensity of narrow-band absorption and wide-band absorption can be dynamically tuned by changing the Fermi level of graphene. Huang[30] *et al*. proposed a tunable wideband terahertz absorber, by which the absorption can be dynamically tuned from 4% to 100% by varying the conductivity of VO$_2$, achieving near-perfect amplitude modulation.

　　Based on the phase change characteristics of VO$_2$, a bi-functional metamaterial absorber with switchable wide-band and narrow-band absorption is proposed in this paper, and the wide-band and narrow-band absorption characteristics of this absorber can be tuned by changing the conductivity of VO$_2$. When VO$_2$ is in the metallic state, the structure is a wide-band absorber consisting of the top layer formed by the metal split ring resonator and VO$_2$ disc, the upper polyimide (PI) dielectric layer, and the VO$_2$ film. When VO$_2$ is in an insulating state, the structure is mainly a narrow-band absorber consisting of the top layer formed by the metal split ring resonator and VO$_2$ disc, the upper PI dielectric layer, the VO$_2$ film, the lower PI dielectric layer, and the metal substrate. Due to the high symmetry of the designed cell structure, the absorber also has the characteristics of insensitivity in polarization and incidence angles over a wide-range, which greatly reduces the limitations of the absorber in the practical application process. The wide- and narrow-band switchable bi-functional absorber proposed in this paper can provide new research ideas for multifunctional tunable devices in terahertz and other frequency bands.

2　Structure and methodology

　　The cell structure of the terahertz metamaterial absorber[28-32] is shown in Figure 1 (Color online), which shows the three-dimensional structure, top view and side view of the periodic cell of the absorber, respectively. The cell structure from top to bottom is a top pattern consisting of a metal split ring resonator and VO$_2$ disc, an upper PI dielectric layer, a VO$_2$ thin film, a lower PI dielectric layer, and a metal substrate, and the device structure is
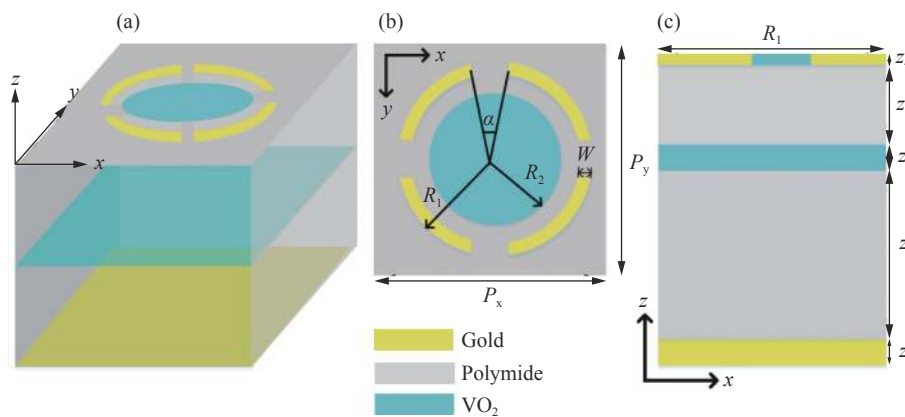

Fig. 1　The absorber (a) 3D schematic; (b) top view; (c) side view

图 1　(a) 吸收器三维示意图;(b) 顶部视图;(c) 侧视图

symmetric about the x and y axes. The resonant structure of the absorber is composed of a metal split ring resonator and a VO_2 disc placed in the center. The calculated optimal geometrical parameters are the period of the structural cell $P_x = P_y = 80$ μm, the ring opening angle $\alpha = 30°$, the outer radius of the split ring $R_1 = 64$ μm, the width of the ring $W = 2$ μm, the radius of the VO_2 disc $R_2 = 47$ μm, the relative permittivity of the upper PI dielectric layer $\varepsilon = 2.0$, the loss angle tangent $\tan\delta = 0.02$[33], and the thickness $Z_3 = 18$ μm, the thickness of the VO_2 film $Z = 1.5$ μm, and the thickness of the lower PI dielectric $Z_1 = 45$ μm. And the metal substrate of the ground plane is a gold material with a thickness of $Z = 1$ μm and a conductivity of $\sigma(\text{gold}) = 4.09 \times 10^7$ S/m[33].

In this paper, the absorption characteristics of the designed switchable metamaterial absorber are numerically simulated by CST software. Terahertz waves are incident on the absorber along $-z$ direction perpendicular to the absorber surface, and the electric field of the incident wave is polarized along x direction and the magnetic field is polarized along y direction. The periodic boundary conditions are used in x and y directions, and the open boundary condition is used in the z direction. The Drude model[2] $\varepsilon(\omega) = \varepsilon_\infty - \dfrac{\omega_p^2(\sigma)}{\omega^2 + i\omega\gamma}$ is used to describe the optical properties of VO_2 in the terahertz frequency range, where $\varepsilon_\infty = 12$ is the high-frequency relative permittivity, $\omega_p(\sigma)$ is the plasma frequency with respect to the conductivity, σ is the conductivity of VO_2, $\gamma = 5.75 \times 10^{13}$ rad/s is the collision frequency, and both $\omega_p(\sigma)$ and σ are proportional to the free carrier density. The relationship between the plasma frequency and conductivity of VO_2 can be approximated as $\omega_p^2(\sigma) = \dfrac{\sigma}{\sigma_0}\omega_p^2(\sigma_0)$, where $\sigma = 3 \times 10^5$ S/m, $\omega_p^2(\sigma_0) = 1.4 \times 10^{15}$ rad/s. By applying the excitation of external electric field, optical field, or temperature field, the phase transition process of VO_2 can occur in a short time. The variation range of conductivity before and after the phase change of VO_2 is about 200 S/m~2×10^5 S/m. By changing the con-

ductivity of VO_2, the wide-band and narrow-band absorption functions of the absorber can be switched. When VO_2 is in the metallic (or insulating) state, its conductivity is 2×10^5 S/m (or 200 S/m)[30], and these two conditions are used to simulate the phase change process of VO_2 in the paper. In the practice, the phase change process of VO_2 can be achieved by changing the temperature. Under thermally excited conditions, the phase transition temperature of VO_2 is approximately 68 ℃. At room temperature, VO_2 is in the insulating state; when the temperature is heated from low to high temperature (over 68 ℃), the molecular structure of VO_2 changes and VO_2 converts from the insulating state to the metallic state; the process is reversible and VO_2 converts from the metallic state to the insulating state when the temperature decreases from the phase change temperature (68 ℃).

3   Results and discussion

The designed metamaterial bi-functional absorber is simulated by using the commercial electromagnetic analysis software CST Microwave Studio. The reflection coefficient (S_{11}) and transmission coefficient (S_{21}) of this absorber are obtained through simulation, then the electromagnetic absorption rate (A) of this structure can be calculated from the following equation:

$$A = 1 - R - T - R_\perp = 1 - |S_{11}|^2 - |S_{21}|^2 - R_\perp \quad , \quad （1）$$

where $R = |S_{11}|^2$ and $T = |S_{21}|^2$ are the reflectance and transmittance obtained from the frequency-dependent S-parameters, and the reflection $R_\perp$ of the cross-polarized wave is also discussed here. In the studied terahertz frequency range, the transmission (T) of the overall metamaterial structure is always 0 due to the presence of metal plates or metallic VO_2 films at the bottom in both states, and the thickness of the metal plates or VO_2 films is much larger than the skin depth of the electromagnetic waves, thus suppressing the transmission. The reflection and absorption spectra of VO_2 with different conductivit-

ies are shown in Fig. 2(a) and Fig. 2(b). When the conductivity changes from 200 S/m to 2×10^5 S/m, the corresponding absorption changes from narrow-band absorption to wide-band absorption, achieving a perfect switch between wide and narrow-band absorption functions.
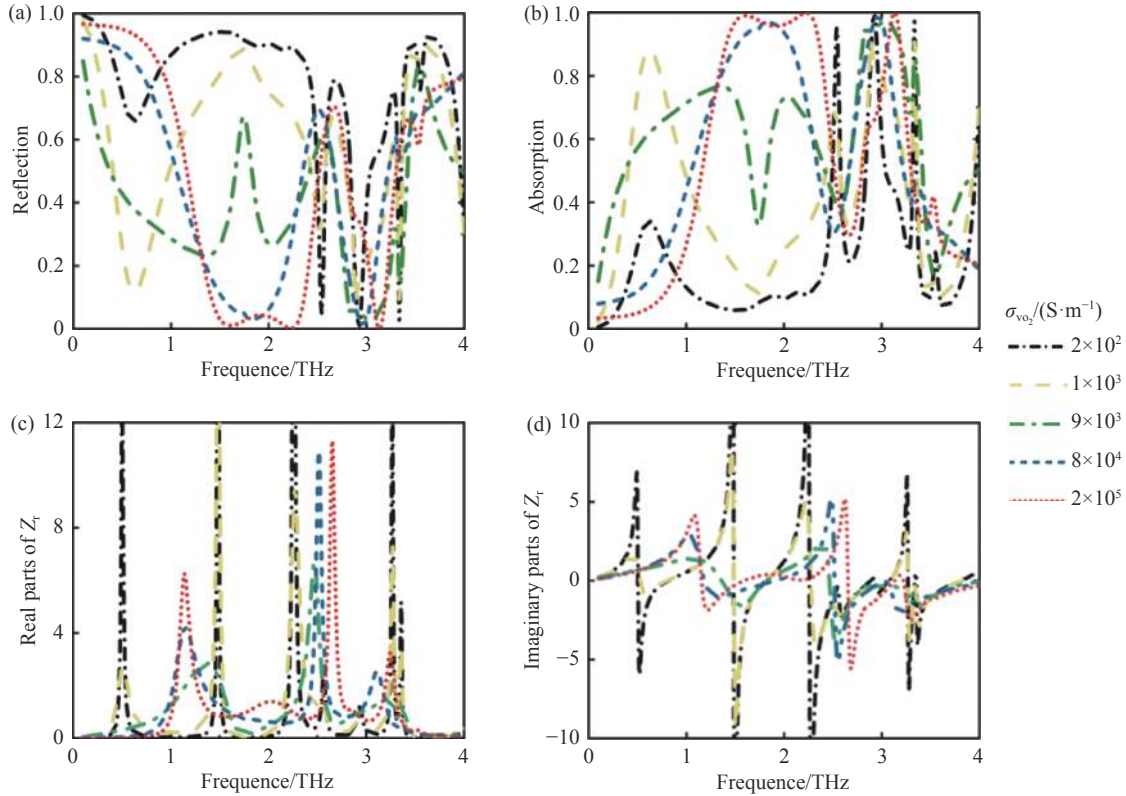

Fig. 2 (a) Reflection spectrum; (b) absorption spectrum; (c) real part of and (d) imaginary part of the relative impedance with different conductivities of VO_2

图 2   二氧化钒不同电导率时的 (a) 反射光谱;(b) 吸收光谱;(c) 相对阻抗的实部和 (d) 虚部

When terahertz wave is incident perpendicular to the device surface, we introduce impedance matching theory to elucidate the intrinsic mechanism for the absorber′s changes. Both the real and imaginary parts of the relative impedance of the absorber can be derived from the *S*-parameter inversion method. The absorption rate and relative impedance can be expressed as[34-35]:

$$A(\omega) = 1 - R(\omega) = 1 - \left|\frac{Z - Z_0}{Z + Z_0}\right|^2 = 1 - \left|\frac{Z_r - 1}{Z_r + 1}\right|^2 , \tag{2}$$

$$Z_r = \pm \sqrt{\frac{(1 + S_{11}(\omega))^2 - S_{21}^2(\omega)}{(1 - S_{11}(\omega))^2 - S_{21}^2(\omega)}} , \tag{3}$$

where Z_0 and Z are the effective impedances of the free space and the absorber, respectively. And

$Z_r = Z/Z_0$ is the relative impedance between the absorber and the free space. The absorption of the wide-band absorber reaches the maximum when the impedance of the absorber matches the impedance of the free space, i.e., the relative impedance of the structure $Z_r=1$. The variation of the real and imaginary parts of the relative impedance for different VO_2 conductivities is shown in Fig. 2 (c) and (d). Obviously, with the continuous increase of the conductivity, the real part gradually approaches to 1 while the imaginary part gradually approaches to 0 in the range of 1.34~2.25 THz, which means that the effective impedance of the absorber and the free space gradually match each other. When VO_2 is in the metallic state, i.e., $\sigma(VO_2) = 2\times10^5$ S/m, the designed structure obtains the highest absorption rate

and the widest absorption bandwidth at the same time.

3.1 Metamaterials can be used as wide-band absorbers when VO₂ is in the metallic state

When VO$_2$ is in metallic state, the designed switchable metamaterial can be used as a wide-band absorber, which consists of a metal split ring resonator on top embedded in a VO$_2$ disc, an upper PI medium, and a VO$_2$ film. When the VO$_2$ is in the metallic state, the bottom metallic phase VO$_2$ acts as the reflection layer, which can prevent the occurrence of transmission. The structural parameters are shown in Fig. 1, and the absorber model is simulated by the finite element method, applying the cell boundary conditions to the x and y boundary conditions and the open boundary in z direction, with the terahertz wave incident along $-z$ direction. The reflection and absorption spectra, as well as the real and imaginary parts of the relative impedance of the wide-band absorber are given in Figure 3 (Color online) when the conductivity of VO$_2$ is 2×10^5 S/m (metallic state), where $A(\omega)$ denotes the absorption spectrum, $R(\omega)$ denotes the reflection spectrum, and Re(Z_r) and Im(Z_r) represent the real and imaginary parts of the relative impedance of the wide-band absorber, respectively. Two different absorption peaks can be observed at 1.53 THz and 2.12 THz, and the designed structure can absorb more than 90% of the energy in the frequency range from 1.34 to 2.25 THz with a bandwidth ratio ($f_{max}-f_{min}$)/[($f_{max}-f_{min}$)/2][37] of 50%. And the absorption in the frequency range from 1.10 to 3.18 THz is greater than 50%, and the corresponding bandwidth ratio is 97%. As shown in Fig. 1(a), the introduction of the top VO$_2$ disc changes the effective impedance of the structure, and the incident electromagnetic waves are better matched with the free space, which also enhances the overall absorption performance of the structure. Therefore, in the wide frequency range of 1.53~2.12 THz, the designed wide-band absorber achieves impedance matching with the free space and obtains a better absorption and wider bandwidth.
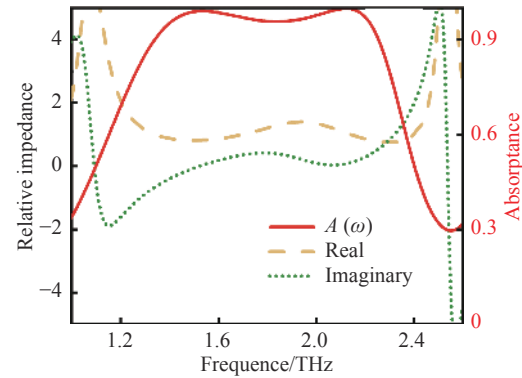

Fig. 3   Reflection and absorption spectra, real part and imaginary part of relative impedance when the conductivity of vanadium dioxide is 2×10^5 S/m

图 3   二氧化钒电导率为 2×10^5 S/m 时反射和吸收光谱、相对阻抗的实部、虚部

In general, the geometric parameters of the structure have an influence on its resonant frequency and absorption rate. Also, errors can be introduced in the structural dimensional parameters during the device processing. Therefore, the structural parameters of the device were investigated. The variation of the terahertz absorption spectrum of the device with the geometric parameters (α, Z_3, R_2) was studied under the condition that the other parameters were kept constant as initial settings, and the results are shown in the following figures. From Fig. 4(a), it can be seen that the absorption bandwidth increases with the increase of the opening angle α. The center frequency of 1.84 THz shows a slight blue-shift trend with the increase of α. The resonance peak at the frequency of 1.53 THz remains basically unchanged, and the resonance peak at the frequency of 2.12 THz shows a blue-shift trend, therefore, the absorption bandwidth increases and the absorption rate decreases with the increase of the opening angle α. In Fig. 4(b), the intensity of the absorption peak first decreases slightly with the increase of Z_3 and reaches the optimum absorption at 18μm, and then the absorption decreases with the increase of Z_3. In Fig. 4(c), the absorption bandwidth changes less with the increase of the radius R_2 of VO$_2$ disc, and the absorption rate decreases slightly, and the best absorption rate is obtained at

47 μm, and the absorption curve shows a blue-shift trend when the radius increases from 44 μm to 47 μm. In summary, it can be seen that the effect of the

change in the opening angle on the absorption bandwidth is more significant than that of the dielectric layer thickness and the radius of the VO$_2$ disc.
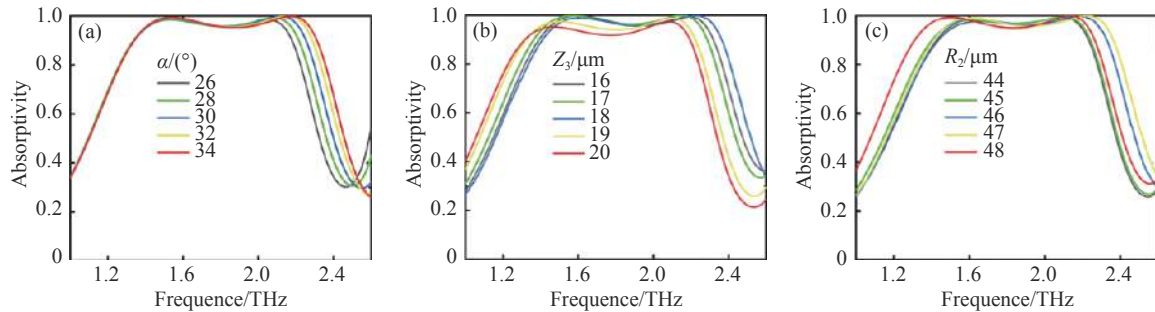

Fig. 4　The influence of the structural parameters of the absorber cell: (a) the opening angle α; (b) the thickness of the upper PI medium Z_3 and (c) the radius of the VO$_2$ disk R_2 on the terahertz absorptivity at the conductivity of 2×10⁵ S/m

图 4　当电导率为 2×10⁵ S/m 时，吸收器单元结构参数对太赫兹吸收率的影响。(a) 开口角度 α；(b) 上层 PI 介质厚度 z_3；(c) VO$_2$ 圆盘半径 R_2

To further understand the operating mechanism of the wide-band absorber in detail, we have studied the electric field distribution at the two resonant frequencies of the wide-band absorber, 1.53 THz and 2.12 THz, as shown in Figure 5. Figure 5 gives the electric field distribution of the absorber at 1.53 THz and 2.12 THz when the incident terahertz wave is transverse electric (TE) polarized, from which it can be seen that the electric fields at the two frequency points are mainly distributed at the two ends of the opening of the metal split ring resonator, the VO$_2$ disc near the opening of the metal ring and along *y*-direction; and the electric field intensity at the frequency of 2.21 THz is more concentrated compared with the induced electric field intensity at the frequency of 1.53 THz. In addi-

tion, the electric field intensity is gradually weakened along the inner edge of the VO$_2$ disc parallel to *x*-axis and near the opening of the metal ring, which may be caused by the weak dipole resonance of the VO$_2$ disc in parallel to *x*-axis near the opening of the metal ring. Due to the structural symmetry, the results of the electric field distribution of the wideband absorber at the above two frequency points exhibit an overall 90° rotation when the incident wave is TM-polarized.

For the needs of absorbers in practical applications, polarization angle insensitivity and incidence angle insensitivity are two very important characteristics. Figure 6(a) (Color online) shows the variation of the absorption performance of the metamaterial absorber with the incident terahertz wave frequency and the incident angle in the TE mode. According to the calculated results, the designed absorber still exhibits a stable absorption rate and a wide operating bandwidth in the large incident angle range of 0°~60°, leading to a high incident angle tolerance. When the incidence angle is larger than 60°, the main absorption peak becomes narrower as the incidence angle increases. Therefore, the absorber can still provide good absorption characteristics even at larger incidence angles. In addition, for TM polarization, the absorption performance remains
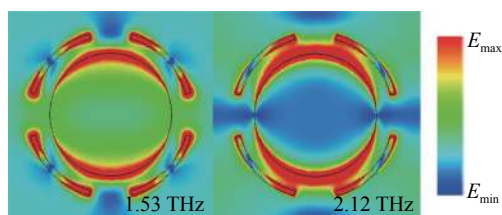

Fig. 5　Electric field intensity distribution at the two absorption peak frequencies of 1.53 THz and 2.12 THz under TE mode

图 5　1.53 THz、2.12 THz 在 TE 极化下两个吸收峰频率处的电场强度分布

stable up to 8° as shown in Fig. 6(b) (Color online). When the incidence angle is larger than 8°, the absorption bandwidth becomes narrower and some higher order modes appear. A similar dependence of the absorption spectrum on the incidence angle was observed in the previously reported VO_2-based absorber[36]. Therefore, the absorption performance of TE polarization is superior to that of TM polarization. The effect of the polarization characteristics of the incident terahertz wave on the absorption performance was also investigated. Figure 6(c) (Color online) shows the absorption rate vs. frequency as

the polarization angle varies from 0° to 90° when a terahertz wave is incident vertically on the absorber surface. It can be seen from Fig. 6(c) that the absorption curves of this wide-band absorber are highly overlapping, i.e., the absorption rate of the absorber is completely independent of the polarization under normal incidence conditions, which is highly related to the symmetry of the absorber cell structure in x and y directions, and the large incidence angle and polarization insensitivity characteristics show high potential for applications in energy harvesting and optical sensing.
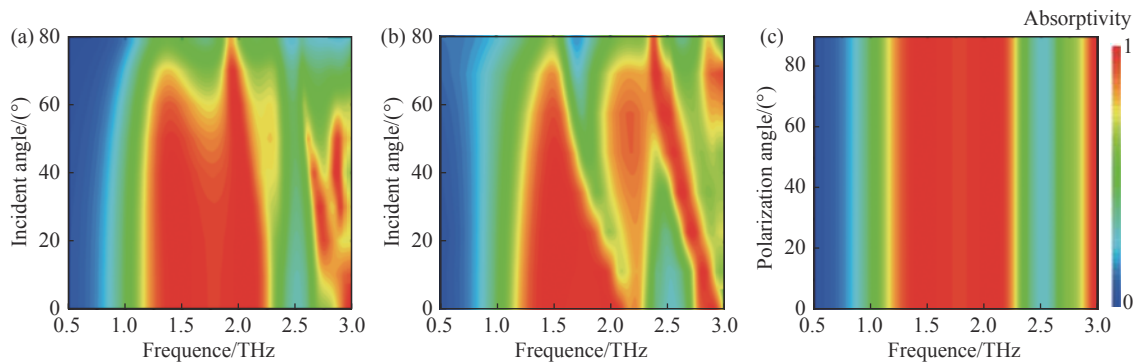

Fig. 6 (a) The absorption of the wide-band absorber with TE polarization at different incident angles; (b) the absorption of the wide-band absorber with TM polarization at different incident angles; (c) the absorption spectrum of the wide-band absorber with different polarization angles; at the conductivity of $2×10^5$ S/m

图 6 当电导率为 $2×10^5$ S/m 时 (a) 不同入射角度时, TE 极化的宽带吸收器的吸收率; (b) 不同入射角度时, TM 极化的宽带吸收器的吸收率; (c) 不同极化角时宽带吸收器的吸收光谱图

3.2 Metamaterials can be used as narrow-band absorbers when VO_2 is in the insulated state

When VO_2 is in the insulating state, the structure of a multi-band absorber consists of a metal split ring resonator on top embedded in a VO_2 disc, an upper PI dielectric, a VO_2 film, a lower PI dielectric, and a metal substrate. The simulation study is performed by using the numerical simulation method of electromagnetic field, and the three-peak absorption spectrum of the multiband absorber can be achieved. Figure 7 shows the reflection and absorption spectra as well as the real and imaginary parts of the relative impedance of the narrow-band absorber at a VO_2 conductivity of 200 S/m. Three absorption peaks exist in the frequency range from 2.4 THz to 4 THz with the resonance frequencies of

2.54 THz, 2.93 THz, and 3.34 THz, the corresponding absorption of 96%, 99.9%, and 99.3%, and the corresponding Full Width at Half Maximum (FWHM)[37] of 93.6 GHz, 206.7 GHz, and 39 GHz, respectively, achieving overall perfect multiband absorption. It can also be seen from Fig. 7 that the real part of the impedance gradually approaches to 1 and the imaginary part gradually approaches to 0 near the multiband absorption peak. The designed multiband narrow-band absorbers achieve the impedance matching between the narrow-band absorber and the free space near the resonant frequencies of 2.54 THz, 2.93 THz, and 3.34 THz.

Under the condition that other parameters remain unchanged as initial settings, the effect of the geometric parameters ($α$, Z_1, W) on the absorption
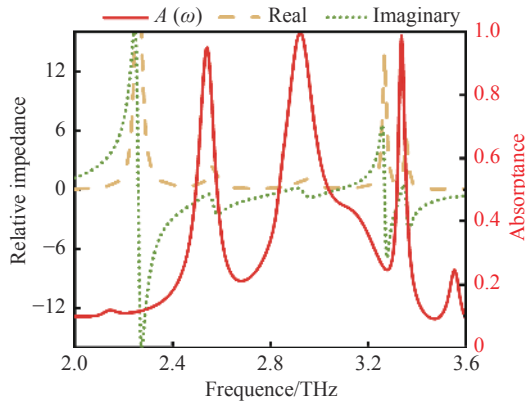
Fig. 7　Reflection and absorption spectra, real part and imaginary part of relative impedance when the conductivity of vanadium dioxide is 200 S/m

图 7　二氧化钒电导率为 200 S/m 时反射和吸收光谱、相对阻抗的实部、虚部

rate was studied, and the calculated results are shown in Figure 8. In Fig. 8(a), the absorption intensity increases significantly with the increase of the opening angle (α), which has a significant effect on the absorption rate at the resonance frequency of 2.54 THz; the absorption rate decreases gradually with the increase of the opening angle at the resonance frequency of 2.93 THz, while the absorption intensity remains unchanged at the resonance frequency of 3.34 THz. In Fig. 8(b), the thickness of the lower PI medium (Z_1) increases from 44 μm to 48 μm in steps of 1 μm, which has a significant effect on the absorption peaks at 2.93 THz and 3.34 THz, and the absorption rate decreases. The strongest absorption intensity is achieved when Z_1 is 45 μm, after which the overall absorption intensity decreases slightly with the increase of Z_1. In Fig. 8 (c), the intensity of the absorption peak first increases with the width of the metal split-ring (W), and the absorption peak in the middle frequence band is more affected, and the strongest absorption peak is obtained at W=2 μm, after which the overall absorption intensity decreases with the increase of W. In summary, it can be seen that the effect of the opening angle is more significant than that of the dielectric layer thickness and the width of the metal split-ring on the absorption bandwith.
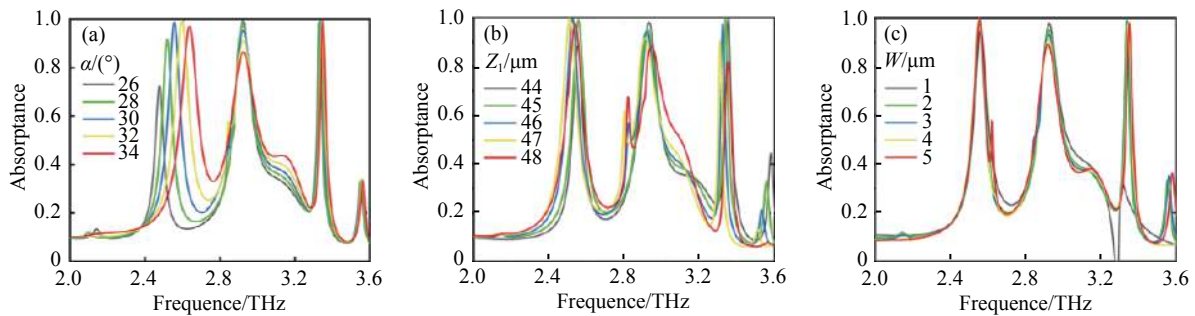

Fig. 8　The influence of the structural parameters of the absorber cell: (a) the opening angle; (b) the thickness of the lower PI medium Z_1 and (c) the width of the metal split ring resonator W, on the terahertz absorption at the conductivity of 200 S/m.

图 8　当 σ 为 200 S/m 时, 吸收器单元结构参数对太赫兹吸收率的影响; (a) 开口角度 (b) 下层 PI 介质厚度 Z1; (c) 金属开口谐振环的宽度 W 而变化

In addition, the electric field intensity distribution at the three absorption peak frequencies of 2.54, 2.93 and 3.34 THz under TE mode is shown in Fig. (9). At 2.54 THz, the electric field distribution is highly concentrated along the two opening-ends of the metal split ring resonator; at 2.93 THz, some energy is uniformly distributed in the center region of the absorber cell; at 3.34 THz, the electric field intensity is strong on both sides of the opening of the metal split ring resonator and within the center region of the absorber cell structure. Due to the symmetry of the structure, the results of the electric field distribution of the narrow-band absorber at the above three frequency points exhibit an overall 90° rotation when the incident wave is TM-polarized.
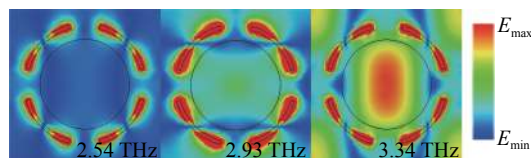
Fig. 9 Electric field intensity distributions at the three absorption peak frequencies of 2.54 THz, 2.93 THz and 3.34 THz under TE mode

图 9 2.54 THz、2.93 THz 和 3.34 THzTE 极化时三个吸收峰频率的电场强度分布

Next, the absorption characteristics of this multiband metamaterial absorber at different polarization angles were also investigated. Fig. 10 depicts the variation of the absorption and frequency when the polarization angle is increased from 0° to 90° in steps of 5°. The results show that the absorption performance of the proposed multiband metamaterial absorber in TE mode does not change with the variation of the incident terahertz wave polarization angle when the terahertz wave is incident vertically on the absorber surface, and its absorption curves are highly coincident. The insensitivity to the polarization angle is related to the symmetry of the absorber cell structure in x and y directions. The intrinsic reason for the symmetry of the designed structure ensures the polarization insensitivity at normal incidence, which is very helpful in many applications.

The structures described in this paper can be processed by molecular beam epitaxy. In 2016, Bi-
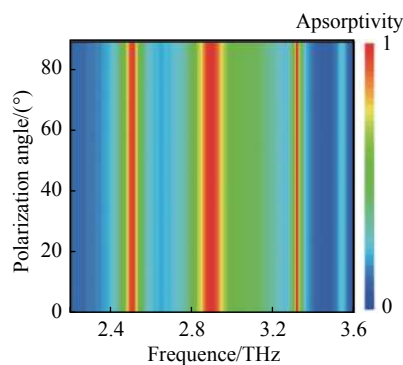

Fig. 10 Absorption spectra of narrow-band absorbers with different polarization angles at the conductivity of 200 S/m

图 10 当电导率为 200 S/m, 不同极化角时窄带吸收器的吸收光谱图

an et al.[38] used molecular beam epitaxy to grow VO$_2$ films on single-crystal sapphire substrates that can be precisely controlled in thickness. In 2017, Sun Hongjun et al.[39] used molecular beam epitaxy to grow a high-quality stoichiometric VO$_2$ films on single-crystal sapphire substrates, and achieved precise control of the film thickness through this technique. For this structure, molecular beam epitaxy can be used to deposit thin VO$_2$ films on PI substrates, and then introduce the disc structure to the top of the VO$_2$ film. Then, metal microstructures are prepared on PI by the conventional lithography and metallization processes to form metallic split ring resonators. The design method proposed in this study provides a new way to study multifunctional components based on continuous VO$_2$ films with completely different functions integrated into one structure.

The terahertz wide-band absorber designed in this paper can be mainly applied to stealth and functional measurements. By absorbing terahertz waves and reducing the energy returned to the detector thus achieving stealth, which can be applied to radar detection, modern warfare weapons and other occasions. The wide-band absorber can be also applied to the field of terahertz wave energy collection and measurement, and the absorber can convert the absorbed energy into electrical energy thus realizing energy measurement.

4 Conclusion

In this paper, a switchable bi-functional metamaterial absorber with wide and narrow bands characteristics is designed, which consists of a top layer pattern composed of a metal split ring resonator and a VO$_2$ disc, an upper PI dielectric layer, a VO$_2$ thin film, a lower PI dielectric layer and a bottom metal substrate, and can be excited by external electromagnetic fields, optical fields and temperature fields to cause the VO$_2$ to undergo an insulating state-metallic state reversible phase transition process, so that the switching between di-

fferent functions can be realized. The switchable structure is numerically simulated in the frequency range of 0~4 THz by the finite element method. The results show that the structure can achieve the function of a high-performance terahertz wide-band absorber with the absorption of 98% in the wide-band frequency range of 1.55 THz to 2.21 THz when VO_2 is in the metallic state. When VO_2 is converted from the metallic state to the insulating state, this structure can realize the multi-band narrow-band absorber. The designed metamaterial absorber can achieve narrow-band absorption above 95% at the resonant frequencies of 2.54 THz, 2.93 THz, and 3.34 THz. In addition, the effects of geometric parameters on the absorption perform-ance are discussed. The absorber device also shows good absorption performance at large incidence angles due to the polarization insensitivity caused by the symmetric structure. The proposed metama-terial absorber with simple structure, switchable function and perfect absorption can be applied to terahertz optical switches, electromagnetic stealth, modulation, thermal emitters and electromagnetic energy harvesting.

——中文对照版——

1　引　言

太赫兹波（THz 波），主要指频率在 0.1 THz 到 10 THz 之间的电磁波，位于微波与红外光波之间[1]。近年来，随着太赫兹探测技术以及时域光谱技术的快速发展，太赫兹波的检测和调制等相关技术受到了越来越多的关注[2]。超材料是一种新型人工设计的电磁复合材料，在太赫兹吸收器[3-4]、极化转换器[5]、传感器[6] 等诸多潜在应用引起了科学界的极大兴趣。近年来，许多研究者已提出了多种基于太赫兹的超材料吸收器模型，并研究了它们的单频带[7]、多频带[8-10] 和宽频带[11-12] 特性。超材料吸收器作为一种对入射的电磁波能实现高吸收率的功能器件[13-14]，其在红外探测[15]、现代通信、电磁隐身[16]、热辐射、传感[17] 等诸多领域具有广阔的应用前景[18-19]。早期的太赫兹吸收器共振模式单一，吸收谱的带宽较窄，大多数设计的超材料吸收器件在工作频率下仅能实现单一的功能或是无法根据应用需求进行吸收性能的调谐，种种缺点都限制了它的实际应用。

随着石墨烯[20-21]、液晶 (LC)[22]、二氧化钒（VO_2）[23] 等功能材料 (相变材料) 的出现，只需要施加电[24-25]、磁、光[26] 以及温度[27] 等激励就能够改变材料的特性。将这些功能材料与超材料结构相结合，就可以在单个超材料器件中实现多个功能，从而推动了太赫兹超材料吸收器的迅速发展。VO_2 作为一种优良的相变材料，其光学和电特性在相变过程中可发生显著变化，电导率可以发生 4~5 个数量级[23] 的改变，因而非常适合用于可调性多功能超材料器件的设计。Liu[23] 等人提出了一种基于 VO_2 超宽带吸收器，可以在 1.2~3.2 THz的宽带范围内实现 5%~80% 吸收率的调制。Song[28] 等人提出了一种基于 VO_2 的太赫兹宽带可调吸收器的设计，当 VO_2 电导率从 10 S/m 变化至 2 000 S/m 时，宽频吸收带的幅值可从 5% 调整至 96%。Zhang[29] 等人提出了一种基于石墨烯间隔/VO_2 间隔/金属结构的具有宽带和窄带吸收特性的太赫兹双功能吸收器，通过改变石墨烯的费米能级，可以动态地调整窄带吸收和宽带吸收的工作带宽和强度。Huang[30] 等人提出了一种可调谐的宽带太赫兹吸收器，通过改变 VO_2 的电导率，可以实现吸收率从 4% 到 100% 的动态调谐，实现了近似完美的振幅调制。

本文基于 VO_2 的相变特性，提出了一种宽、窄带吸收可切换的双功能超材料吸收器，可以通过改变 VO_2 材料的电导率，实现该吸收器的宽、窄带吸收特性调控。当 VO_2 处于金属状态时，该结构为金属开口谐振环和 VO_2 圆盘形成的顶层、上层聚酰亚胺 (PI) 介质层、VO_2 膜组成的宽带吸收器。当 VO_2 处于绝缘状态时，结构主要为金属开口谐振环和 VO_2 圆盘形成的顶层、上层 PI 介质层、VO_2 膜、下层 PI 介质层、金属衬底组成的窄带吸收器。由于所设计的单元结构具有高度对

称性,该吸收器还具有极化不敏感和宽入射角度范围内不敏感的特性,大大降低了吸收器在实际应用过程中的局限。本文的宽、窄带可切换的双功能吸收器可为太赫兹和其他频段的多功能可调器件提供新的研究思路。

2　结构与方法

太赫兹波(THz 波),超材料吸收器[28-32]的单元结构如图 1(彩图见期刊电子版)所示,图 1(a)~1(c)分别展示了吸收器的周期性单元三维立体结构、俯视图和侧视图。该单元结构从上到下依次是金属开口谐振环和 VO$_2$ 圆盘构成的顶层图案、上层 PI 介质层、VO$_2$ 薄膜、下层 PI 介质层、金属衬底,器件结构关于 x 和 y 轴对称。吸收器的谐振结构是由金属开口谐振环和中心放置一块 VO$_2$ 圆盘组成。经计算得到最优的几何参数,其中结构单元的周期 P_x=P_y=80 μm,圆环开口角度 α=30°,开口圆环外半径 R_1=64 μm,圆环宽度 W=2 μm,VO$_2$ 圆盘半径 R_2=47 μm,上层 PI 介质的相对介电常数为 ε=2.0,损耗角正切值为 $\tan\delta$=0.02[33],厚度为 Z_3=18 μm。VO$_2$ 薄膜的厚度 Z=1.5 μm,下层 PI 介质厚度 Z_1=45 μm,接地面的金属衬底为金材料,其厚度为 Z=1 μm,电导率为 σ(gold)=4.09×10^7 S/m[33]。

本文使用 CST 软件对设计的可切换超材料吸收器的吸收特性进行数值仿真研究。太赫兹波垂直表面沿$-z$ 方向入射到吸收器上,入射波的电场沿 x 方向极化,磁场沿 y 方向极化;x 和 y 方向设置为单元周期边界,z 方向为开放边界条件。采用 Drude 模型[2]$\varepsilon(\omega)=\varepsilon_\infty-\dfrac{\omega_p^2(\sigma)}{\omega^2+i\omega\gamma}$来描述太赫兹频率范围 VO$_2$ 的光学性质,其中ε_∞=12 为高频相对介电常数,$\omega_p(\sigma)$ 为与电导率有关的等离子体频率,σ 为 VO$_2$ 的电导率,γ=5.75×10^{13} rad/s 为碰撞频率,且 $\omega_p(\sigma)$ 和 σ 都与自由载流子密度成正比。VO$_2$ 的等离子体频率与电导率关系可以近似地表示为:$\omega_p^2(\sigma)=\dfrac{\sigma}{\sigma_0}\omega_p^2(\sigma_0)$,其中 σ=3×10^5 S/m,$\omega_p^2(\sigma_0)$=1.4×10^{15} rad/s。通过施加外部电场、光场、温度场的激励可使 VO$_2$ 在较短时间内发生相变过程。改变 VO$_2$ 的电导率可切换吸收器的宽带和窄带吸收功能。VO$_2$ 相变前后电导率的变化范围大约为 200 S/m~2×10^5 S/m,通过改变

VO$_2$ 的电导率可切换吸收器的宽带和窄带吸收功能。当 VO$_2$ 处于金属(或绝缘)状态时,其电导率为 2×10^5 S/m(或 200 S/m)[30],文中利用这两个条件来模拟 VO$_2$ 的相变过程。在应用中,VO$_2$ 的相变过程可以通过改变温度来实现。在热激励条件下,VO$_2$ 材料的相变温度大概为 68 ℃。当温度为室温时,VO$_2$ 处于绝缘态;当温度从低温加热到高温时(超过 68 ℃),VO$_2$ 材料的分子结构发生变化,VO$_2$ 从绝缘态变为金属态;该过程是一可逆过程,当温度从相变温度(68 ℃)以上降低到相变温度以下时,VO$_2$ 从金属态转换为绝缘态。

3　结果与讨论

使用商用电磁分析软件 CST Microwave Studio 对所设计的超材料双功能吸收器进行仿真,得到该吸收器的反射系数(S_{11})和透射系数(S_{21}),则该结构的电磁吸收率(A)可以由以下公式计算:

$$A=1-R-T-R_\perp=1-|S_{11}|^2-|S_{21}|^2-R_\perp \quad,（1）$$

其中,R=$|S_{11}|^2$ 和 T=$|S_{21}|^2$ 是从与频率相关的 S 参数获得的反射率和透射率,这里还需讨论交叉极化波的反射 $R_\perp$。在所研究的太赫兹频率范围内,由于两种状态下底部都有金属板或者金属态的 VO$_2$ 薄膜存在,且金属板或 VO$_2$ 薄膜的厚度远远大于电磁波的趋肤深度,因而抑制了透射部分,超材料整体结构的透射(T)始终为 0。VO$_2$ 电导率不同时的反射和吸收光谱如图 2(a) 和图 2(b) 所示。当电导率从 200 S/m 变为 2×10^5 S/m 时,相应的吸收从窄带吸收转变成为宽带吸收,实现了完美宽、窄带吸收功能的切换。

当太赫兹垂直于器件表面入射时,引入了阻抗匹配理论来阐明吸收器发生变化的内在机理。吸收器的相对阻抗的实部虚部均可由 S 参数反演法导出。吸收率和相对阻抗可表示成[34-35]:

$$A(\omega)=1-R(\omega)=1-\left|\frac{Z-Z_0}{Z+Z_0}\right|^2=1-\left|\frac{Z_r-1}{Z_r+1}\right|^2,\quad（2）$$

$$Z_r=\pm\sqrt{\frac{(1+S_{11}(\omega))^2-S_{21}^2(\omega)}{(1-S_{11}(\omega))^2-S_{21}^2(\omega)}}.\quad（3）$$

其中,Z_0 和 Z 分别是自由空间和吸收器的有效阻抗。而 Z_r=Z/Z_0 则是吸收器与自由空间之间

的相对阻抗，当吸收器的阻抗与自由空间的阻抗相匹配时，即结构的相对阻抗 $Z_r=1$ 时，宽带吸收器的吸收率达到最大值。如图 2(c) 和 2(d) 显示了不同 VO_2 电导率时相对阻抗的实部和虚部的变化情况。显然，随着电导率不断地增加，在 1.34~2.25 THz 范围内，实部逐渐接近于 1 的同时虚部逐渐接近于 0，这意味着吸收器的有效阻抗和自由空间的有效阻抗之间逐渐匹配。当 VO_2 处于金属态时，即 $\sigma(VO_2)=2\times10^5$ S/m 时，所设计结构同时获得了最高的吸收率和最宽的吸收带宽。

3.1 金属态时超材料可作为宽带吸收器

当 VO_2 处于金属态时，设计的可切换超表面可以用作宽带吸收器，其由顶部金属开口谐振环嵌入一块 VO_2 圆盘、上层 PI 介质、VO_2 薄膜组成. 当 VO_2 处于金属态时，底部金属相 VO_2 作为反射层，可以阻止透射的发生。结构参数如图 1 所示，采用有限元方法对吸收器模型进行模拟，将单元格边界条件应用于 x 和 y 边界条件，并在 z 方向开放边界，入射太赫兹沿着 $-z$ 方向入射。图 3（彩图见期刊电子版）给出了 VO_2 电导率为 2×10^5 S/m(金属态) 时宽带吸收器的反射、吸收光谱以及相对阻抗的实部、虚部。其中 $A(\omega)$ 表示吸收光谱，$R(\omega)$ 表示反射光谱，$Re(Z_r)$ 和 $Im(Z_r)$ 分别代表了宽带吸收器相对阻抗的实部和虚部。在 1.53 THz 和 2.12 THz 可以观察到 2 个不同的吸收峰，在 1.34~2.25 THz 频率范围内，所设计的结构可吸收 90% 以上的能量，带宽比 $(f_{max}-f_{min})/[(f_{max}-f_{min})/2]$[37] 为 50%，在 1.10~3.18 THz 频率范围内的吸收率大于 50%，相应的带宽比为 97%。其中如图 1(a)所示，顶层 VO_2 圆盘的引入改变了结构的有效阻抗，入射的电磁波与自由空间更加匹配，这也增强了结构整体的吸收性能。因此在 1.53~2.12 THz 的宽频范围内，所设计的宽带吸收器与自由空间实现了阻抗匹配，获得了较优的吸收和较宽的带宽。

一般来说，结构的几何参数对其共振频率和吸收率有一定的影响。同时，在器件加工过程中，也会在结构尺寸参数上引入误差。因此，本文对器件的结构参数进行了研究。在其他参数作为初始设置保持不变的情况下，研究了器件的太赫兹吸收谱随几何参数(α、Z_3、R_2)的变化规律，研究

结果如图 4（彩图见期刊电子版）所示。由图 4(a) 可以看出，吸收带宽随着开口角度 α 的增加而增大，中心频率 1.84 THz 随着 α 的增大呈轻微蓝移趋势，频率为 1.53 THz 处的谐振峰基本保持不变，频率为 2.12 THz 处的谐振峰呈蓝移趋势，由此得知，随开口角度 α 的增加，吸收带宽增大，吸收率降低。在图 4(b) 中，吸收峰强度首先随着 Z_3 的增加而略微减少，在 18 μm 达到最佳吸收率，而后吸收率随着 Z_3 的增加而减小。在图 4(c) 中，随着 VO_2 圆盘半径 R_2 的增加吸收带宽变化较小，吸收率略有下降，在 47 μm 处获得最佳的吸收率，并且当半径从 44 μm 增加到 47 μm 时，吸收曲线呈蓝移趋势。综上所述，与介质层厚度和 VO_2 圆盘半径的影响相比，开口角度的变化对吸收带宽的影响效果更为显著。

为了进一步详细了解宽带吸收器的工作机理，研究了该宽带吸收器两个共振频率 1.53 THz 和 2.12 THz 处的电场分布，如图 5 所示。图 5 给出了入射太赫兹波为 TE 极化时吸收器在 1.53 THz 和 2.12 THz 处的电场分布。从图中可以看出，两个频率点处的电场主要分布在金属开口谐振环的开口两端、VO_2 圆盘靠近金属圆环开口处且沿着 y 轴方向；且相较于 1.53 THz 频率处的感应电场强度，2.21 THz 频率处的电场强度更为聚集；此外，电场强度沿着 VO_2 圆盘在与 x 轴平行且靠近金属圆环开口的内边缘逐渐减弱，这可能是由于 VO_2 圆盘在与 x 轴平行靠近金属圆环开口的弱偶极子共振引起的。由于结构设计的对称性，入射波为 TM 极化时宽带吸收器在上述两个频率点处的电场分布整体展现出 90° 的旋转。

针对吸收器在实际应用中的需求，极化角度不敏感和入射角度不敏感性是非常重要的两大特性。图 6(a)（彩图见期刊电子版）给出了在横电(TE)模式下，超材料吸收器吸收性能随入射太赫兹波频率以及入射角度的变化规律。根据计算结果，所设计的吸收器在 0°~60°大入射角范围内仍展现出稳定的吸收率和较宽的工作带宽，具有较高的入射角容忍能力。当入射角大于 60°时，其主吸收峰随着入射角的增大而变窄。因此，该吸收器即使在较大的入射角下，仍然能够提供较好的吸收特性。此外，对于 TM 极化，如图 6(b)（彩图见期刊电子版）所示，吸收性能保持在 8°以内

的稳定。当入射角大于 8°时,吸收带宽变窄,出现了一些高阶模态。在先前报道的基于 VO_2 的吸收器[36]中也观察到吸收光谱对入射角的类似依赖性。因此,TE 极化的吸收性能优于 TM 极化。同时还研究了入射太赫兹波的极化特性对吸收性能的影响。图 6(c)(彩图见期刊电子版)给出了当太赫兹波垂直入射到吸收器表面时,极化角从 0°变化到 90°时的吸收率和频率的关系。从图 6(b) 可以看出,该宽带吸收器的吸收曲线是高度重合的,即在正常入射条件下,吸收器的吸收率与极化是完全无关的,这与吸收器单元结构在 x 和 y 方向上的对称性有着很大关系,大入射角度和极化不敏感特性在能量采集和光学传感中展现出较高的应用潜力。

3.2 绝缘态时超材料可作为窄带吸收器

当 VO_2 为绝缘态时,该结构由顶部金属开口谐振环嵌入一块 VO_2 圆盘、上层 PI 介质、VO_2 薄膜、下层 PI 介质、金属衬底组合构成多频带吸收器。采用电磁场数值模拟方法进行模拟研究,可得多频带吸收器的三峰吸收谱,图 7 展示了 VO_2 电导率为 200 S/m 时窄带吸收器的反射、吸收光谱图以及相对阻抗的实部、虚部。可见,在 2.4 THz~4 THz 频率范围内存在 3 个吸收峰,其共振频率分别为 2.54 THz、2.93 THz 和 3.34 THz,对应的吸收率分别为 96%、99.9% 和 99.3%,对应半高宽 (FWHM)[37] 分别为 93.6 GHz、206.7 GHz 和 39 GHz,整体实现了多频带的完美吸收。从图 6 中还可看出,在多频吸收峰附近,阻抗实部逐渐接近于 1,虚部逐渐接近 0。在 2.54 THz、2.93 THz、3.34 THz 共振频率附近所设计的多频窄带吸收器都实现了窄带吸收器与自由空间之间的阻抗匹配。

固定其他参数的初始设置不变,研究几何参数(α、z_1、W)对吸收率产生的影响,计算结果如图 8(彩图见期刊电子版)所示。图 8(a) 中,随着开口角度 (α) 的增大吸收强度明显增加,对共振频率 2.54 THz 处的吸收率影响较为显著;在共振频率 2.93 THz处,吸收率随着开口角度的增大而逐渐减小,而在 3.34 THz 共振频率处吸收强度保持不变。在图 8(b) 中,下层 PI 介质厚度 (z_1) 从 44 μm 以 1 μm 为步长变化增加至 48 μm,对于 2.93 THz 和 3.34 THz 处的吸收峰变化影响较大,

吸收率有所降低。z_1 在 45 μm 处达到最佳吸收曲线,之后随 z_1 的增加整体吸收强度略有减小。在图 8(c) 中,随着金属开口环宽度 (W) 的增加,中间频带的吸收峰所受到的影响较大,在 2 μm 处获得最佳的吸收曲线,之后随着 W 的增加整体吸收强度反而减小。综上可看出,与介质层厚度和金属开口环宽度的影响相比,开口角度的影响效果更为显著。

此外,本文还研究了 2.54 THz、2.93 THz 和 3.34 THz 3 个吸收峰频率处的电场强度分布,如图(9)所示,给出了 TE 极化太赫兹波入射时 3 个吸收峰频率处的电场分布。在 2.54 THz 处,电场分布沿着金属开口谐振环的开口两端高度集中;在 2.93 THz 处,有部分能量均匀分布在吸收单元中心区域;在 3.34 THz 处,金属开口谐振环的开口两侧、吸收器单元结构中心区域范围内的电场强度很强。由于结构设计的对称性,入射波为 TM 极化时,窄带吸收器在上述 3 个频率点处的电场分布的结果整体展现了 90°的旋转。

接下来,还研究了该多频带超材料吸收器在不同极化角度下的吸收特性。图 10 描述了极化角从 0°以 5°的步长增加到 90°时吸收率与频率的变化规律。结果表明,TE 模式下,当太赫兹波垂直入射到吸收器表面,本文中所提出的多频带超材料吸收器的吸收性能不随入射太赫兹波极化角度的变化而改变,其吸收曲线是高度重合的。极化角度的不敏感性与吸收器单元结构在 x 和 y 方向上的对称性有关。所设计结构的对称性这一内在原因确保了在正常入射下的极化不敏感性,这在许多应用中非常有帮助。

本文结构可以采用分子束外延法进行加工。2016 年,Bian 等人[38]利用分子束外延技术在单晶蓝宝石基底上生长可以精确控制厚度的 VO_2 薄膜。2017 年,孙洪君等人[39]采用分子束外延技术在单晶蓝宝石衬底上生长了高质量化学计量比 VO_2 薄膜,通过该技术实现了薄膜厚度的精确控制。就本结构而言,可采用分子束外延在 PI 衬底上沉积薄 VO_2 薄膜,再将圆盘结构引入到 VO_2 薄膜的顶部。然后,在传统的光刻和金属化工艺的基础上,在 PI 上制备金微结构,形成金属 CSRRS。本研究提出的设计方法为以连续 VO_2 薄膜为基础,将完全不同的功能集成到一个结构中的多功

能元器件的研究提供了新的途径。

　　本文所设计的太赫兹宽带吸收器主要可以应用于隐身和功能测量等方面。通过吸收太赫兹波,降低返回探测器的能量从而实现隐身,可以应用在雷达探测、现代战争武器等场合。同时,宽带吸收器可以应用于太赫兹波能量收集、测试计量领域,吸收器可以将吸收的能量转换为电能量从而实现能量测量。

4　结　论

　　本文设计了一种具有宽、窄频带特性的可切换双功能超材料吸收器,该吸收器由金属开口谐振环和 VO_2 圆盘构成的顶层图案、上层 PI 介质层、VO_2 薄膜、下层 PI 介质层和底部金属衬底构成,通过外部电磁场、光场以及温度场等激励,可以使 VO_2 发生绝缘态-金属态可逆相变过程,从而可以实现不同功能之间的转换。采用有限元方法对该可切换结构在 0~4 THz 频段进行数值模拟,结果表明：当 VO_2 处于金属态时,此结构可以实现高性能太赫兹宽带吸收器功能,在 1.55 THz~2.21 THz 的频率范围内可实现 98% 的宽带吸收。当 VO_2 从金属态转换为绝缘态时,此结构可以实现多频带窄带吸收器功能,所设计的超材料吸收器的共振频率为 2.54 THz、2.93 THz、3.34 THz 时,窄带吸收率在 95% 以上。此外,还讨论了几何参数对吸收率性能的影响。该吸收器件由于对称结构产生了极化不敏感性能,在大入射角时也表现出良好的吸收性能。本文提出的超材料吸收器具有结构简单、可切换功能和完美吸收等特性,可应用于太赫兹光电开关、电磁隐身、调制、热发射器和电磁能量采集等场合。

References:

[1]　鲍迪, 沈晓鹏, 崔铁军. 太赫兹人工电磁媒质研究进展[J]. 物理学报, 2015, 64(22)：228701.
　　　BAO D, SHEN X P, CUI T J. Progress of terahertz metamaterials[J]. *Acta Physica Sinica*, 2015, 64(22)：228701.(in Chinese)

[2]　SONG ZH Y, WEI M L, WANG ZH SH. Terahertz absorber with reconfigurable bandwidth based on isotropic vanadium dioxide metasurfaces[J]. *IEEE Photonics Journal*, 2019, 11(2)：4600607.

[3]　XU R J, LIU X Y, LIN Y SH. Tunable ultra-narrowband terahertz perfect absorber by using metal-insulator-metal microstructures[J]. *Results in Physics*, 2019, 13: 102176.

[4]　CHEN L, LIAO D G, GUO X G, *et al.*. Terahertz time-domain spectroscopy and micro-cavity components for probing samples: a review[J]. *Frontiers of Information Technology & Electronic Engineering*, 2019, 20(5)：591-607.

[5]　LI CH Y, CHANG C C, ZHOU Q L, *et al.*. Resonance coupling and polarization conversion in terahertz metasurfaces with twisted split-ring resonator pairs[J]. *Optics Express*, 2017, 25(21)：25842-25852.

[6]　LEE Y, KIM S J, PARK H, *et al.*. Metamaterials and metasurfaces for sensor applications[J]. *Sensors*, 2017, 17(8)：1726.

[7]　LANDY N I, SAJUYIGBE S, MOCK J J, *et al.*. Perfect metamaterial absorber[J]. *Physical Review Letters*, 2008, 100(20)：207402.

[8]　SHAN Y, CHEN L, SHI CH, *et al.*. Ultrathin flexible dual band terahertz absorber[J]. *Optics Communications*, 2015, 350: 63-70.

[9]　WEN Q Y, ZHANG H W, XIE Y S, *et al.*. Dual band terahertz metamaterial absorber: design, fabrication, and characterization[J]. *Applied Physics Letters*, 2009, 95(24)：241111.

[10]　BAO ZH Y, WANG J CH, HU ZH D, *et al.*. Coordinated multi-band angle insensitive selection absorber based on graphene metamaterials[J]. *Optics Express*, 2019, 27(22)：31435-31445.

[11]　方晓敏, 江孝伟, 武华. 双波长窄带宽介质超材料吸收器[J]. 中国光学, 2021, 14(6)：1327-1340.
　　　FANG X M, JIANG X W, WU H. Dual-wavelength narrow-bandwidth dielectric metamaterial absorber[J]. *Chinese Optics*, 2021, 14(6)：1327-1340.(in Chinese)

[12]　ZHANG Y B, LIU W W, LI ZH CH, *et al.*. Ultrathin polarization-insensitive wide-angle broadband near-perfect absorber in the visible regime based on few-layer MoS_2 films[J]. *Applied Physics Letters*, 2017, 111(11)：111109.

[13]　CHEN SH Q, CHENG H, YANG H F, *et al.*. Polarization insensitive and omnidirectional broadband near perfect planar metamaterial absorber in the near infrared regime[J]. *Applied Physics Letters*, 2011, 99(25)：253104.

［14］ KONG H, LI G F, JIN Z M, *et al*.. Polarization-independent metamaterial absorber for terahertz frequency［J］. *Journal of Infrared, Millimeter, and Terahertz Waves*, 2012, 33（6）: 649-656.

［15］ RYZHII V, OTSUJI T, RYZHII M, *et al*.. Graphene terahertz uncooled bolometers［J］. *Journal of Physics D: Applied Physics*, 2013, 46（6）: 065102.

［16］ SCHURIG D, MOCK J J, JUSTICE B J, *et al*.. Metamaterial electromagnetic cloak at microwave frequencies［J］. *Science*, 2006, 314（5801）: 977-980.

［17］ WANG Y, CUI Z J, ZHU D Y, *et al*.. Multiband terahertz absorber and selective sensing performance［J］. *Optics Express*, 2019, 27（10）: 14133-14143.

［18］ 张检发, 袁晓东, 秦石乔. 可调太赫兹与光学超材料［J］. 中国光学, 2014, 7（3）: 349-364.
ZHANG J F, YUAN X D, QIN SH Q. Tunable terahertz and optical metamaterials［J］. *Chinese Optics*, 2014, 7（3）: 349-364.（in Chinese）

［19］ 任智慧, 钟绵增, 杨珏晗, 等. 基于AsP/MoS₂异质结的偏振光电探测器［J］. 中国光学, 2021, 14（1）: 135-144.
REN ZH H, ZHONG M Z, YANG J H, *et al*.. A polarization-sensitive photodetector based on a AsP/MoS$_2$ heterojunction［J］. *Chinese Optics*, 2021, 14（1）: 135-144.（in Chinese）

［20］ 袁莹辉, 陈飚宇, 胡放荣, 等. 基于人工超表面/离子凝胶/石墨烯复合结构的太赫兹调幅器件［J］. 中国激光, 2019, 46（6）: 0614016.
YUAN Y H, CHEN X Y, HU F R, *et al*.. Terahertz amplitude modulator based on metasurface/ion-gel/graphene hybrid structure［J］. *Chinese Journal of Lasers*, 2019, 46（6）: 0614016.（in Chinese）

［21］ WEIS P, GARCIA-POMAR J L, RAHM M. Towards loss compensated and lasing terahertz metamaterials based on optically pumped graphene［J］. *Optics Express*, 2014, 22（7）: 8473-8489.

［22］ WU Y, RUAN X ZH, CHEN C H, *et al*.. Graphene/liquid crystal based terahertz phase shifters［J］. *Optics Express*, 2013, 21（18）: 21395-21402.

［23］ LIU H, WANG ZH H, LI L, *et al*.. Vanadium dioxide-assisted broadband tunable terahertz metamaterial absorber［J］. *Scientific Reports*, 2019, 9（1）: 5751.

［24］ HU F R, WANG H, ZHANG X W, *et al*.. Electrically triggered tunable terahertz band-pass filter based on VO₂ hybrid metamaterial［J］. *IEEE Journal of Selected Topics in Quantum Electronics*, 2019, 25（3）: 4700207.

［25］ QAZILBASH M M, BREHM M, CHAE B G, *et al*.. Mott transition in VO₂ revealed by infrared spectroscopy and nano-imaging［J］. *Science*, 2007, 318（5857）: 1750-1753.

［26］ HALLMAN K A, MILLER K J, BAYDIN A, *et al*.. Sub-picosecond response time of a hybrid VO₂: silicon waveguide at 1550 nm［J］. *Advanced Optical Materials*, 2021, 9（4）: 2001721.

［27］ YAN D X, MENG M, LI J SH, *et al*.. Vanadium dioxide-assisted broadband absorption and linear-to-circular polarization conversion based on a single metasurface design for the terahertz wave［J］. *Optics Express*, 2020, 28（20）: 29843-29854.

［28］ SONG ZH Y, CHEN A P, ZHANG J H. Terahertz switching between broadband absorption and narrowband absorption［J］. *Optics Express*, 2020, 28（2）: 2037-2044.

［29］ ZHANG M, SONG ZH Y. Terahertz bifunctional absorber based on a graphene-spacer-vanadium dioxide-spacer-metal configuration［J］. *Optics Express*, 2020, 28（8）: 11780-11788.

［30］ HUANG J, LI J N, YANG Y, *et al*.. Broadband terahertz absorber with a flexible, reconfigurable performance based on hybrid-patterned vanadium dioxide metasurfaces［J］. *Optics Express*, 2020, 28（12）: 17832-17840.

［31］ SONG ZH Y, ZHANG J H. Achieving broadband absorption and polarization conversion with a vanadium dioxide metasurface in the same terahertz frequencies［J］. *Optics Express*, 2020, 28（8）: 12487-12497.

［32］ LIU W W, SONG ZH Y. Terahertz absorption modulator with largely tunable bandwidth and intensity［J］. *Carbon*, 2021, 174: 617-624.

［33］ 初启航, 杨茂生, 陈俊, 等. 可调控的太赫兹多频带吸收器特性［J］. 中国激光, 2019, 46（12）: 1214003.
CHU Q H, YANG M SH, CHEN J, *et al*.. Characteristics of tunable Terahertz multi-band absorber［J］. *Chinese Journal of Lasers*, 2019, 46（12）: 1214003.（in Chinese）

［34］ ZHANG CH Y, ZHANG H, LING F, *et al*.. Dual-regulated broadband terahertz absorber based on vanadium dioxide and graphene［J］. *Applied Optics*, 2021, 60（16）: 4835-4840.

［35］ ZHOU R H, JIANG T T, PENG ZH, *et al*.. Tunable broadband terahertz absorber based on graphene metamaterials and

VO$_2$[J]. *Optical Materials*, 2021, 114: 110915.

[36]　CHEN A P, SONG ZH Y. Tunable isotropic absorber with phase change material VO$_2$[J]. *IEEE Transactions on Nanotechnology*, 2020, 19: 197-200.

[37]　PAN W, SHEN T, MA Y, *et al.*. Dual-band and polarization-independent metamaterial terahertz narrowband absorber[J]. *Applied Optics*, 2021, 60(8): 2235-2241.

[38]　BIAN J M, WANG M H, SUN H J, *et al.*. Thickness-modulated metal–insulator transition of VO$_2$ film grown on sapphire substrate by MBE[J]. *Journal of Materials Science*, 2016, 51(13): 6149-6155.

[39]　SUN H J, WANG M H, BIAN J M, *et al.*. Terahertz and metal-insulator transition properties of VO$_2$ film grown on sapphire substrate with MBE[J]. *Journal of Inorganic Materials*, 2017, 32(4): 437-442.

Author Biographics：

FENG Qin-yin (1997 —), Female, from Shaoyang, Hunan Province, China, M.S. student, mainly engaged in research on terahertz metamaterials. E-mail: 1162935753@qq.com

封覃银（1997—），女，湖南邵阳人，硕士研究生，主要从事太赫兹超材料方面的研究。E-mail: 1162935753@qq.com

QIU Guo-hua (1974—), Male, from Shaoxing, Zhejiang Province, China, Ph. D., Lecturer, received his Ph.D. degree from Zhejiang University in 2012, mainly engaged in the research of terahertz sources and devices, Email: qghfr@163.com

裘国华（1974—），男，浙江绍兴人，博士，讲师，2012 年于浙江大学获得博士学位，主要从事太赫兹源及器件研究，Email: qghfr@163.com

YAN De-xian (1991—), Male, from Wuwei, Gansu Province, China, Ph. D., associate professor, received his Ph.D. degree from Tianjin University in 2018, mainly engaged in the research of terahertz sources and devices. E-mail: yandexian1991@cjlu.edu.cn

严德贤（1991—），男，甘肃武威人，博士，副教授，2018 年于天津大学获得博士学位，主要从事太赫兹源及器件研究。E-mail: yandexian1991@cjlu.edu.cn